Surface modification of hydroxyapatite by yttrium ion substitution for adsorption of reactive red dye

G. Vasugi[a], A. Thamizhavel[b], E. K. Girija[a,*]

aDepartment of Physics, Periyar University, Salem 636 011, India
bDepartment of Condensed Matter Physics, Tata Institute of Fundamental Research, Colaba, Mumbai 400 005, India

Abstract

Hydroxyapatite (HA), a calcium phosphate phase with Ca/P ratio 1.67 is well known for its adsorption properties. Here we report a detailed study on the reactive red dye adsorption by nano sized HA and a trivalent cation (yttrium) substituted HA (Y-HA) prepared by simple wet precipitation route. Characterization of synthesized samples using XRD, FT-IR and SEM confirmed the formation of rod like nanoparticles of HA.Y-HA exhibited enhanced adsorption affinity than the pristine HA due to the existence of additional adsorption sites such as O^{2-} and Y^{3+}.Kinetic and isotherm studies revealed pseudo second order kinetics and monolayer adsorption of dye. Thus the adsorption efficiency of HA can be tailoredusing trivalent cation substitution in HA. Regeneration ability, economic preparation and environmental friendly disposal are the advantages of HA.

1. Introduction

20-30 % of textile dyes in the market belongs to the class of reactive dyes. During the process of dyeing, only 70% of it adheres to the textile and 30% remain unfixed thatgets discharged in the effluent [1, 2]. Various decolorization technologies such as biological methods, physical methods, chemical methods and combined physico-chemical methods have been developed to treat dye containing wastewaters. Among them adsorption process is a simple and efficient method for treating organic contaminants from the waste water streams.

Currently expensive activated carbon prepared from different sources is used as the adsorbent for water treatment which is largely restricted to removal of nonpolar materials and shows complexity in regeneration. Hence active research is focused on the design and development of efficient and economic adsorbents which can treat a wide range of dyes [3, 4]. Surface area and surface chemistry of the adsorbents plays an important role for both physisorption and chemisorption. The potential use of nanomaterials for the remediation of contaminated soil, water and air are explored due to their unique reactivity in nano regime. The larger surface area and high accessible adsorption sites of the nanomaterials facilitate adsorption of large amount of pollutants. Presence of more number of unsaturated atoms on the surface that can easily bind with other atoms and short intraparticle diffusion distance of nanomaterials favor the adsorption capacity [5, 6].

Calcium phosphates are known to be good adsorbents for the last six decades [7]. Hydroxyapatite [$Ca_{10}(PO_4)_6(OH)_2$, HA], a calcium phosphate phase with Ca/P ratio 1.67 is widely investigated in biomaterials research for its bioactive characteristics. Its interaction with biological macromolecules such as protein is widely studied for biomedical applications [8]. The excellent adsorption affinity of HA has made it useful for separation, purification of proteins andpurification of blood (for removal of pathogenic proteins)[9]. Adsorption affinity of HA towards many heavy metals such as cadmium, lead and zinc has been studied by Alessia Corami *et al* [10]. Nanocrystalline HA has been identified as a cost effective sorbent for defluoridation of drinking water [11].

An interesting property of apatite is its ability to accept ionic substituents and the vacancies created in its structure as a result of substitutionwhich helps in tailoring the properties of HA including adsorption. Metal ion substitution in HA is an interesting topic of research as adsorption behaviour is merely governed by the surface

structure of the adsorbent. Ionic substitution is found to alter the surface charge and specific surface area of HA plays an important role in the interaction of dye molecule with apatite matrix. The incorporation of transition metals like zinc enhanced the protein adsorption of HA and copper doping improved the arsenide sorption from ground water [12-14]. The excellent adsorption potential of HA caused by material defect and/or substitution are attributed to the difference in bonding site distribution and surface charge density. Rare earth ions doped adsorbents such as TiO_2 and magnetite revealed enhanced adsorption and photocatalytic activity [15,16].In the present work in order to understand the influence of rare earth ion substitution in HA on textile dye removal, we investigated the effect of a trivalent rare earth cation substitution in the structure of HA on the adsorption of reactive red dye from aqueous solution. Yttrium has been chosen as the model trivalent cation for this study.

2. Materials and methods
2.1. Chemicals

Calcium nitrate tetrahydrate $Ca(NO_3)_2.4H_2O$, di-ammonium hydrogen phosphate $(NH_4)_2HPO_4$, yttrium nitrate hexahydrate $Y(NO_3)_3.6H_2O$ and ammonia solution NH_4OH were used as the starting materials. All reagents used for the experiments were GR grade obtained from Merck (INDIA) and used without any further purification. N-cetyl-N,N,N-trimethylammonium bromide ($C_{19}H_{42}BrN$,CTAB) was obtained from Loba chemie. The reactive red 198 dye ($C_{27}H_{18}ClN_7Na_4O_{15}S_5$, RR198) obtained from a textile company was also used without further purification and deionised water was used as the solvent. The molecular structure of reactive red dye is shown in figure 1.
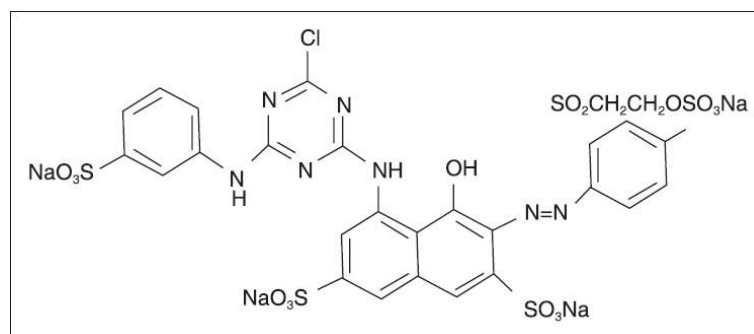

Figure 1: Molecular structure of reactive red 198 dye

2.2. Experimental procedure

Solution A and B containing 1 M of $Ca(NO_3)_2.4H_2O$ and 0.6 M of $(NH_4)_2HPO_4$ with 0.2 M of CTAB respectively were separately brought to pH above 10 by adding ammonia. Solution A was stirred vigorously at room temperature and solution B was added in drops into it. The reaction mixture was stirred for one hour and the suspension was aged for 24 hours. The resultant precipitate was separated from the suspension by centrifuging and washing with water and ethanol. Washed precipitate was dried in hot air oven at 110°Cto obtain the white HA powder. A similar procedure was adopted to synthesize Y-HA, except for the fact that the solution A was prepared with 0.95 M of Ca $(NO_3)_2.4H_2O$ and 0.05 M of Y $(NO_3)_3.6H_2O$.
Adsorption experiment was carried out by batch method and various experiments were carried out to optimize the adsorbent dosage, pH and adsorbate concentration. A predetermined amount of adsorbent (0.05, 0.1, 0.2, 0.3 and 0.4 gm) was added to 25 mL of dye solution of varying concentration from 50 to 250 mg/Lin steps of 50 and the mixture was placed in ashaker incubator (100 rpm) at 37°C. Samples were withdrawn from the shaker at predetermined time intervals and the residual concentration of dye solution was determined spectrophotometrically at λ_{max} (517 nm).Effect of solution pH on dye removal was investigated by changing the initial pH from 2 to 12 in steps of 2 adjusted by using dilute HCl or NH_4OH. All experiments were carried out in triplicate, and the average values were taken to minimise random error.

The amount of dye adsorbed on the adsorbent (mg/g) was calculated using the mass balance equation,

$$q_e = \frac{(c_0 - c_e)V}{W} \qquad (1)$$

where c_0 and c_e are the initial and equilibrium concentrations of dye (mg/L), V is volume of the solution (L) and W is weight of the adsorbent (g).

2.3. Calcium estimation using EDTA-titration

After attaining equilibrium the adsorbent was retrieved from the dye solution by filtration. Amount of calcium ion released from the adsorbent into the dye solution during adsorption was estimated using EDTA titration technique. The filtered dye solution was taken in a conical flask and adjusted to a pH between 12-14 using 4 ml of 8 M NaOH. A small amount of Patton and Reeder indicator was added to the solution and 0.025 M of EDTA was titrated against the dye solution till the end point (colour change from pink to blue) was reached. Then the Ca^{2+} concentration in dye solution was estimated by using the following equation

$$EDTA_{mol} \times V_{EDTA} = Ca^{2+}_{mol} \times V_{Ca}^{2+} \qquad (2)$$

The experiment was repeated three times to get the average value and standard deviation.

2.3. Characterization

The X-ray diffraction (XRD) patterns were obtained using RIGAKU MINI FLEX II diffractometer in the range $20° \leq 2\theta \leq 60°$ with Cu Kα radiation. The FT-IR spectra were recorded in the region 4000 - 400 cm^{-1} using a Perkin Elmer FT-IR spectrometer by KBr pellet technique. The molar concentrations of elements (Ca, P and Y) in the samples were quantified by X-ray Fluorescence (XRF) using JEOL element analyzer. The specific surface area of the samples was determined by Brunauer–Emmett–Teller (BET) method of N_2 adsorption using the Nova Station A Quanta chrome instrument. The morphology of as synthesized samples was examined using FEI Tecnai transmission electron microscope (TEM).The change in the dye concentration was measured by monitoring the absorbance of the supernatant dye solution at λ_{max} (517 nm) using a Perkin Elmer – Lambda 35 UV–Vis spectrophotometer.

3. Results and discussion

Figure 2 (A) and (B) show the powder XRD pattern of pure HA and Y-HA, before and after adsorption. All the observed diffraction peaks matched well with the hexagonal phase of HA (JCPDS File No. 09-0432). Both Y^{3+} ion substitution and dye adsorption did not change the phase except for a small shift in the peak position for Y-HA, which lead to a decrease in the lattice constant *a* and a slight increase in the *c* parameter, with an ultimate decrease in the unit cell volume.
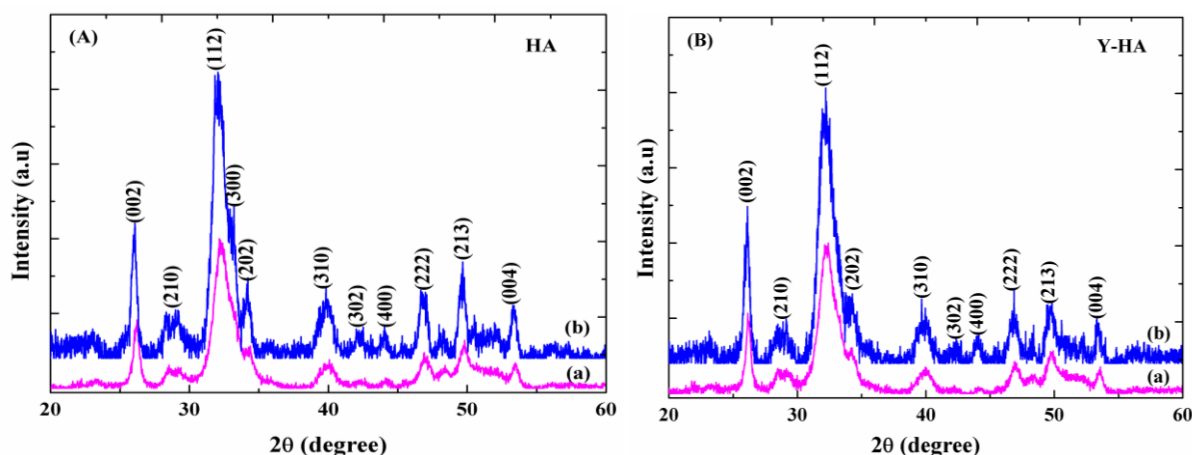

Figure 2: (A) XRD pattern of HA, (B) Y-HA (a) before adsorption (b) after dye adsorption

The crystalline lattice parameters estimated from the XRD of the samples are given in Table 1. The difference in the lattice parameters of Y-HA when compared to HA clearly indicates the substitution of Y^{3+} ions in HA structure. The ionic radius of the yttrium ion (0.90 Å) is less when compared with the ionic radius of calcium ion (1.00 Å) and hence the addition of Y^{3+} results in the formation of more compact structure which results in the reduction of unit cell volume and increase of lattice distortion. The average particle size calculated using the Debye–Scherrer approximation [17] was found to be 46 nm and 51 nm respectively for HA and Y-HA.

Table 1: Crystalline parameters of HA and Y-HA

Adsorbents	Lattice parameters (Å)		Crystallite size D_{hkl} (nm)	Degree of crystallinity x_c	Unit cell volume $V(Å^3)$	Lattice distortion c/a
	$a=b$	c				
HA	9.701	6.792	46	2.515	553.60	0.7001
Y-HA	9.423	6.812	51	3.547	523.95	0.7228

Substitution of a trivalent cation Y^{3+} in place of the divalent cation Ca^{2+} leads to charge imbalance and the possible modes of charge balance can be described as mentioned below. One type of charge balance mechanism resulting due to trivalent yttrium cation substitution for Ca^{2+} is formation of a Ca^{2+} ion vacancy for two Y^{3+} ions as given by equation 3 and another type is that the excessive positive charge introduced by the substitution is compensated by an increase in negative charge via transformation of OH^- ions into O^{2-} ions as given by equation 4 [18-21].

$$2Ca^{2+} \leftrightarrow 2Y^{3+} + V_{Ca} \qquad (3)$$
$$Ca^{2+} + 2OH^- \leftrightarrow Y^{3+} + OH^- + O^{2-} \qquad (4)$$
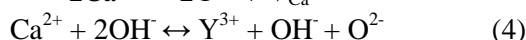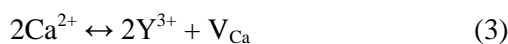
The adsorption property of HA can be thought to be as follows: the site Ca^{2+} is exposed on the crystal surface and contributes to the surface charge and interaction with other organic compounds. Also the surface is rich in negatively charged hydroxyl and phosphate groups which contribute to the surface charge of HA. The vacancies created due to substitution also play an important role in adsorption process. Figure 3 shows the structure of HA and trivalent ion substituted HA. The FT-IR spectra of the RR dye, adsorbents before and after adsorption are shown in figure 4 (a-e). HA exhibited v_3 PO_4^{3-} stretching mode vibration at 1039 cm^{-1} and v_2 PO_4^{3-} bending mode at 473 cm^{-1}.It also exhibited characteristic v_4 PO_4^{3-} bending modes at 568 and 603 cm^{-1}. For HA the characteristic O-H stretching mode is observed at 632 cm^{-1} and 3570 cm^{-1} and the carbonate peak appeared at 1483 cm^{-1}.
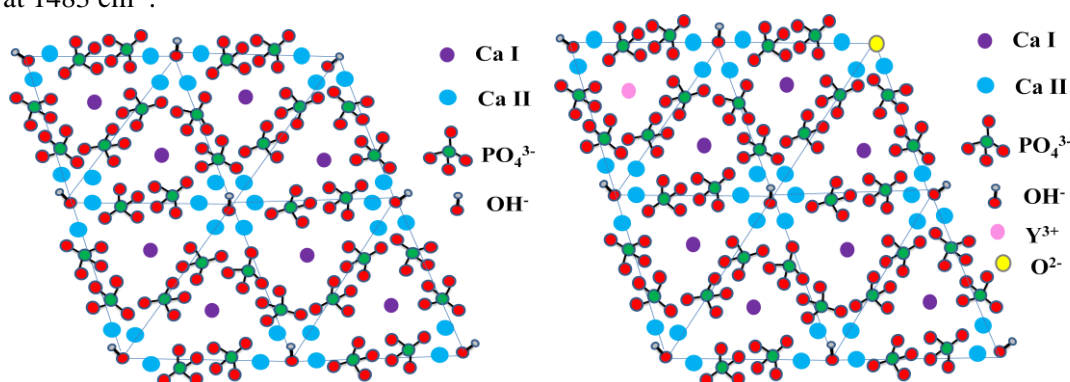
Figure 3: Structure of HA and trivalent ion substituted HA

Yttrium substitution did not produce much change in v_3 and v_4 modes of PO_4^{3-} vibrations. The carbonate bands appeared at 1403 cm^{-1} and 832 cm^{-1}. Absence of OH^- bands at 632 and 3570 cm^{-1} in Y-HA can be attributed to the partial transformation of OH^- ions into O^{2-} ions. The peaks at 1626 cm^{-1} (N=N), 1484 cm^{-1} (C=C), 1405 cm^{-1} (C-H), 1286 cm^{-1} (C-O-C), 1124 cm^{-1}(SO_3^-), 746 cm^{-1} (C-H) and 618 cm^{-1} (C-Cl) are the functional groups of reactive red dye [22]. All the spectra possess a broad band extending from 3400 to 3200 cm^{-1} due to stretching vibrations of O–H groups of adsorbed H_2O. The appearance of peaks belonging to the dye molecule after adsorption clearly indicates the adsorption of dye by the adsorbent.

XRF analysis confirmed the presence of calcium, phosphorus and yttrium in the samples. The molar ratio of Ca/P in HA was found to be 1.6302 and for Y-HA (Ca+Y)/P was 1.7379. The specific surface area (SSA) of the samples by BET method using N_2 adsorption was found to be 85.520 (m²/g) and 110.386 (m²/g) for HA and Y-HA respectively. The significant increase in the specific surface area of Y-HA may be due to the change in the size and shape of nanostructures due to the rare earth ion substitution.
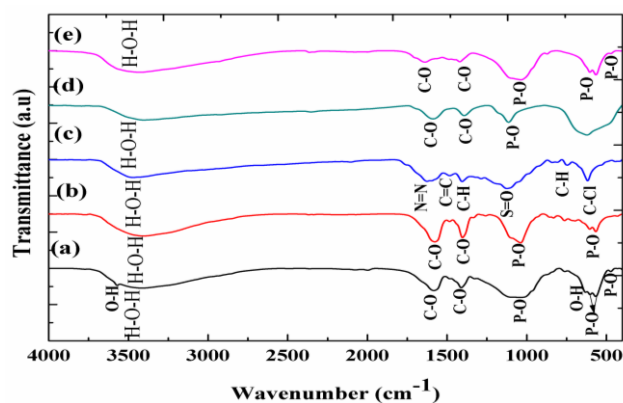
Figure 4: FT-IR Spectra of (a) HA (b) Y-HA (c) reactive red dye (d) HA after dye adsorption (e) Y-HA after dye adsorption

UV absorption measurement of the dye solutions after adsorption did not exhibit shift in λ_{max} but showed only changes in the intensity and the formation of colored adsorbent after contact with the dye solution indicates that the dye molecule is not broken. Thus there is no change in the properties of both adsorbent and adsorbate hence the nature of the observed process is physical adsorption. The TEM and SAED images of samples HA and Y-HA are shown in figures 5(a) and 5(b) respectively. Sample HA exhibits uniform shape and sized short rod or spindle like nanostructures. The TEM images of Y-HA show significant elongation of the rod like particles and aggregation. The SAED pattern of both the samples exhibits continuous rings around the sharp spot which indicates the polycrystalline nature of the samples. The particle length of HA was found to be 34.78 nm whereas Y-HA was 51.64 nm long. Similar type of elongation of rod like HA nanoparticles on trivalent ion substitution was also reported by Kandori et al., [23].
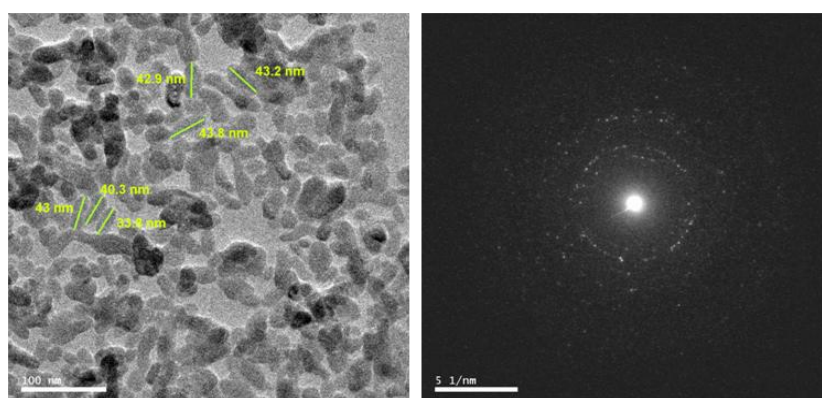

Figure 5(a): TEM image and SAED pattern of HA

Ca^{2+} ion estimation after dye adsorption revealed the presence of 0.1 mM and 0.2 mM Ca^{2+} ions in solutions respectively for HA and Y-HA indicating the dissolution of apatite in the dye solution during adsorption. The increase in the structural disorder due to yttrium ion substitution might be the reason for the increased Ca ion release that caused increased solubility. Also at equilibrium the pH of the supernatant solution of HA and Y-HA incubated samples were found to be 6.8 and 7.03 respectively. The increase in the pH compared to the initial pH of the dye solution is also the consequence of dissolution of apatite during which OH^- ions are released into the solution. The point of zero charge of apatite mineral lies between pH 4 and 9 [24]. Figure 6. shows the effect of pH on percentage of dye removal. HA exhibited better dye removal in acidic pH while Y-HA in the basic pH. Of the different pH studied, pH 6 showed maximum dye removal for both HA and Y-HA. Figure 7 shows the percentage of dye removal obtained for different adsorbent dosages of samples studied at pH 6 and adsorbate concentration of 50 mg/L. The percentage of dye removal increases with increase in adsorbent dosage for both the adsorbents due to the increase in surface area available for adsorption. The maximum dye removal observed for HA was 89% and it was 92% for Y-HA.
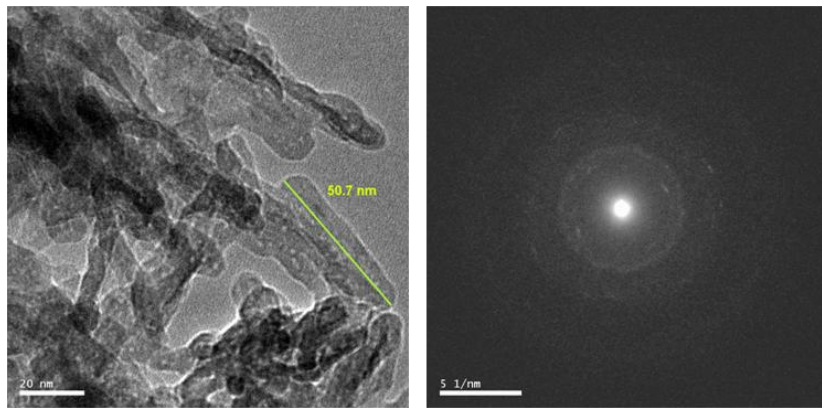
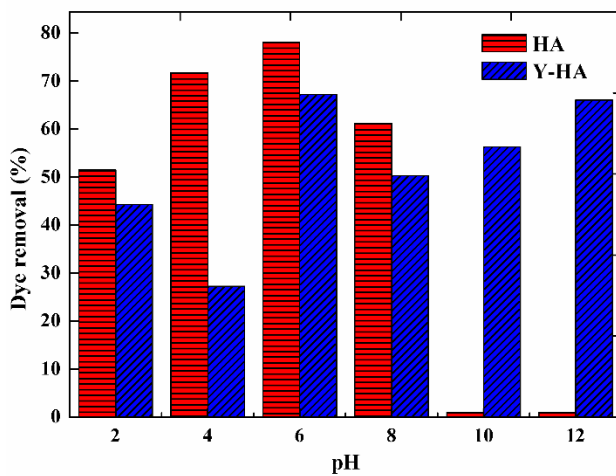**Figure 5(b):** TEM image and SAED pattern of Y-HA

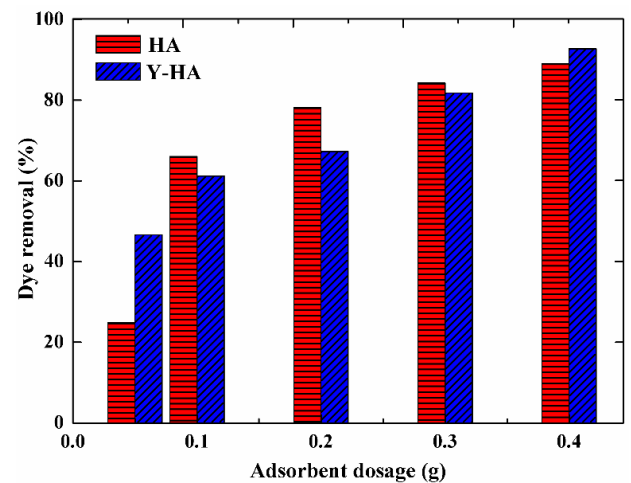**Figure 6:** Effect of pH on percentage of dye removal

Figure 7: Dye removal by HA and Y-HA for various adsorbent dosages

The representative picture obtained for percentage of dye removal at pH 6and 0.2 g of adsorbent for varying adsorbate concentration is given in figure 8. Dye adsorption was maximum for both HA and Y-HA at 150 mg/L and the dye removal decreased due to the unavailability of adsorption sites for increased number of dye molecules. Figure 9 shows the effect of contact time on percentage of dye removal for HA and Y-HA at optimized pH for adsorbent dosage of 0.2 g and adsorbate dosage of 50 mg/L. Percentage of dye removal increases with time and approaches equilibrium above 360 min. The removal of dye is rapid at initial stage for Y-HA than HA.Figure 10. shows the photograph of untreated, HA and Y-HA treated dye solution at equilibrium.
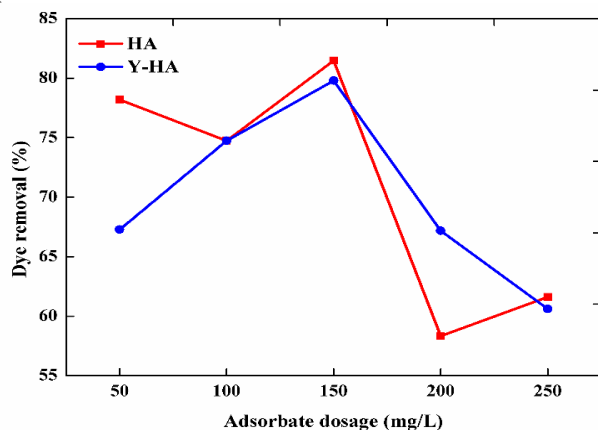

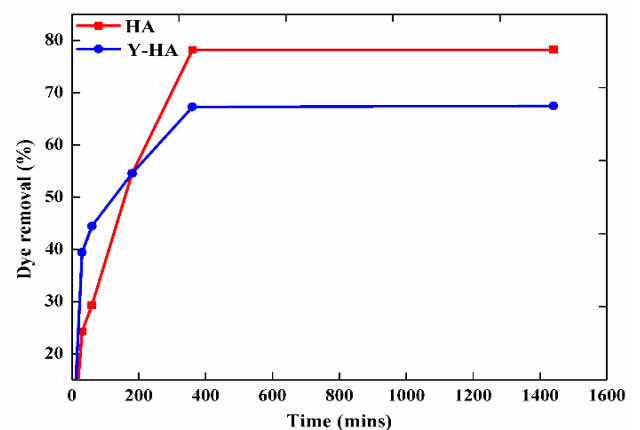**Figure 8:** Dye removal by HA and Y-HA for various adsorbate concentrations

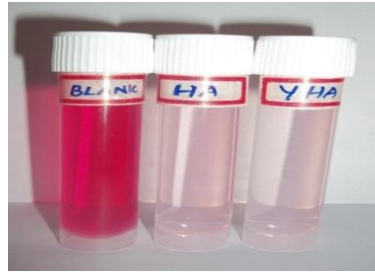**Figure 9:** Effect of contact time on percentage of dye removal

Figure 10: Photograph of untreated and HA, Y-HA treated dye solution.

The most commonly studied adsorption isotherms are Langmuir and Freundlich models. Linearized form of the Langmuir isotherm can be written as

$$\frac{c_e}{q_e} = \frac{1}{q_m} c_e + \frac{1}{K_a q_m} \qquad (5)$$

By this method the values of q_m and K_a were predicted from the slope and the intercept of the plot c_e/q_e vs c_e. The Langmuir constants q_m (mg/g) and K_a (1/mg) represents the adsorption capacity and energy of adsorption respectively. The Freundlich isotherm model can be used for the heterogeneous surface energy systems. This model describes the non-ideal and reversible adsorption, which is not restricted to the formation of monolayer and the linear form is given by,

$$\log q_e = \log K_F + \frac{1}{n} \log c_e \qquad (6)$$

where K_F (mg/g) (l/mg)$^{1/n}$ is the Freundlich constant which indicates the adsorption capacity of the adsorbent and n is a Freundlich exponent related to the intensity of adsorption. By linear regression method the values of $1/n$ and K_F were calculated from the slope and the intercept of the linear plot $\log q_e$ vs $\log c_e$ [25]. The linear plots for Langmuir isotherm model for HA and Y-HA are shown in figure 11.
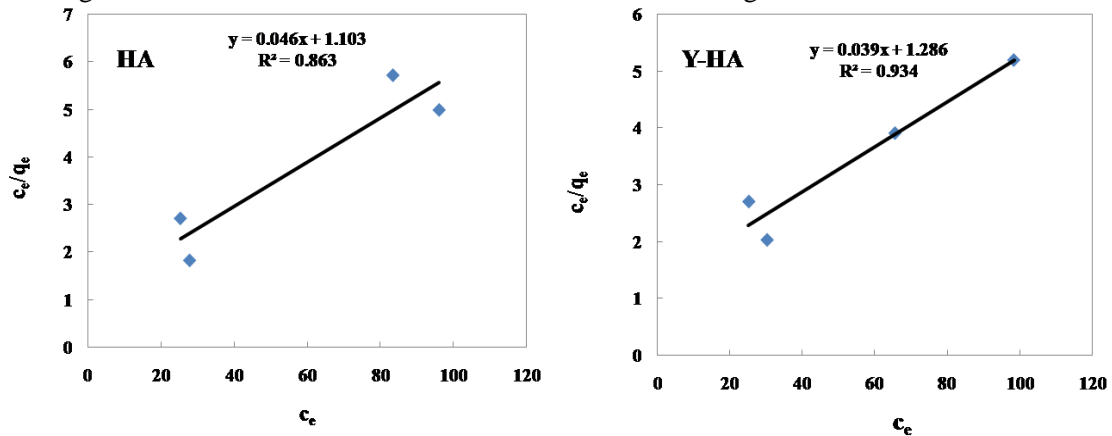

Figure 11: Langmuir adsorption isotherm plots of HA and Y-HA

Table 2: Isotherm model constants and correlation coefficients

Adsorbents	Langmuir Isotherm			Freundlich Isotherm		
	q_m (mg/g)	K_a(l/mg)	r^2	K_F (mg/g) (l/mg)$^{1/n}$	N	r^2
HA	21.4976	0.042	0.863	0.8578	3.2883	0.7101
Y-HA	25.2811	0.030	0.934	0.5339	2.44619	0.8488

The linear form of pseudo first order reaction is given by equation 7,

$$\log(q_e - q_t) = \log q_e - \frac{k_1}{2.303} t \qquad (7)$$

By linear regression analysis the pseudo first order constants q_e and k_1 can be determined from the slope and intercept of the plot log $(q_e - q_t)$ vs t. The linear form of the pseudo second order equation is given by equation 8,

$$\frac{t}{q_t} = \frac{1}{k_2 q_e^2} + \frac{1}{q_e} t \qquad (8)$$

where k_2 (min^{-1}g/mg) is the second order rate constant of sorption which is used to calculate the initial sorption rate. The value of k_2 and the equilibrium adsorption capacity q_e can be calculated from the intercept and slope of the plot t/q_t vs t. The linear plots for pseudo second order model for HA and Y-HA are shown in figure 12.

HA y = 0.202x + 1.360 R² = 0.998

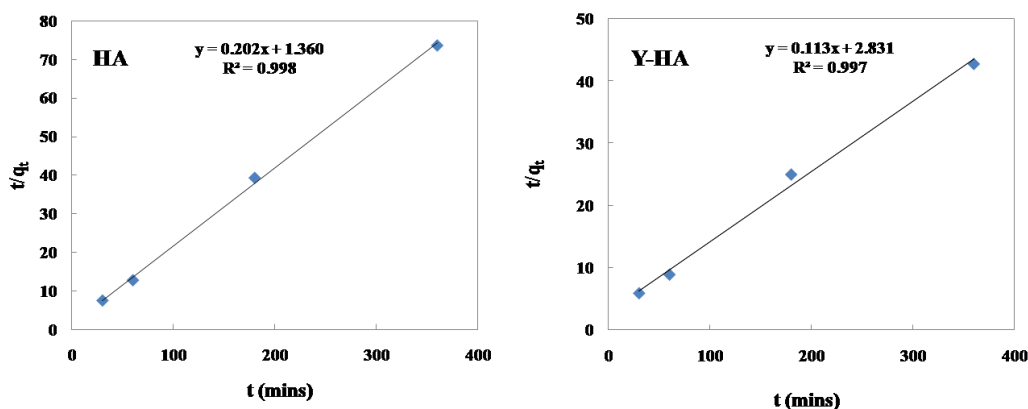Y-HA y = 0.113x + 2.831 R² = 0.997

Figure 12: pseudo second order kinetic plots of HA and Y-HA

From table 2 it is clear that both the samples follow Langmuirian type adsorption which indicates the monolayer adsorption capacity of the adsorbents. The data obtained from kinetic studies given in table 3 reveal that the reaction follows Pseudo second order kinetics.

Table 3: Kinetic model constants and correlation coefficients

| Adsorbents	q_e (mg/g) (exp)	Pseudo first order kinetics			Pseudo second order kinetics		
		q_e (mg/g) (cal)	k_1	r^2	q_e (mg/g) (cal)	k_2	r^2
HA	4.88	2.231	0.003	0.293	4.938	17.91	0.998
Y-HA	8.40	1.442	0.005	0.856	8.837	27.57	0.997

According to the mechanism proposed by Dorozhkin for the dissolution of HA a series of events occur such as diffusion and adsorption of acids from the bulk of the solution onto the surface through the Nernst layer resulting in the chemical transformations on the surface which is followed by desorption and diffusion of reaction products through the Nernst layer to the bulk solution [26, 27]. In the case of HA the dissolution starts with OH$^-$ group followed by Ca^{2+} and finally PO$_4^{3-}$ due to their definite geometrical arrangement in the crystal lattice. Diffusion and adsorption of H$^+$ on the surface leads to the transformation of OH$^-$ of HA into H$_2$O as shown below:

$$Ca_5(PO_4)_3OH + H_2O + H^+ = Ca_5(PO_4)_3(H_2O)^+ + H_2O \qquad (9)$$
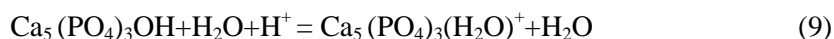
Subsequently the nearest calcium cation is removed and sorption of next proton takes place transforming the protonated HA into TCP and then TCP into Ca cation and monocalcium hydrogen phosphate according to the equation given below:

$$2Ca_5(PO_4)_3(H_2O) = 3Ca_3(PO_4)_2 + Ca^{2+} + H_2O \qquad (10)$$
$$Ca_3(PO_4)_2 + 2H^+ = Ca^{2+} + 2CaHPO_4 \qquad (11)$$
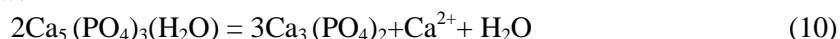
Removal of first PO$_4^{3-}$ group occurs when the third Ca^{2+} ion is released and is given by:

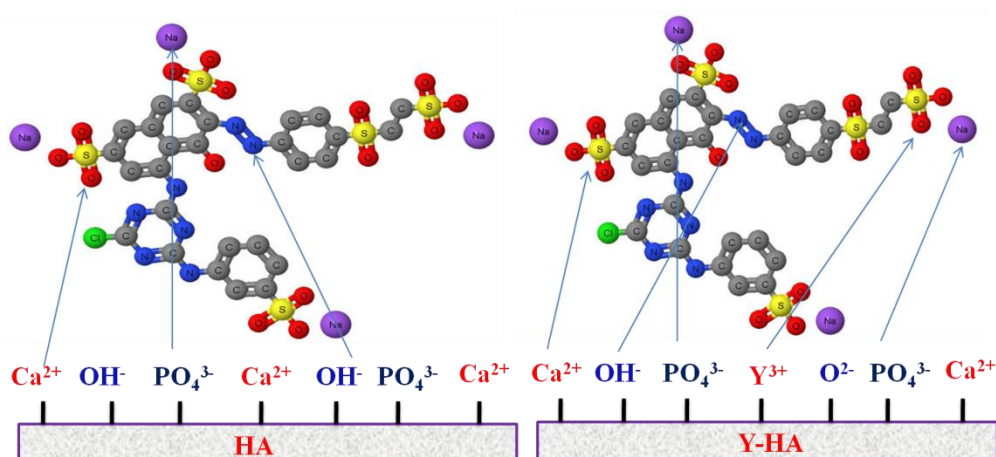$$2CaHPO_4 + 2H^+ = Ca^{2+} + H_3PO_4^- \qquad (12)$$
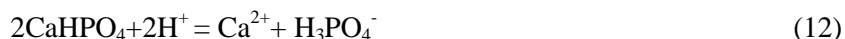
Figure 12: Interaction of reactive red dye with HA and Y-HA

Figure 13 shows the interaction of dye at the surface of HA and Y-HA. The adsorption takes place at the interfacial surface that exists between the two phases. The surfaces of HA ceramics immediately change when exposed to dye solution. At HA surface the dye molecule adsorb through the electrostatic attractions between the ionized sulphonyl groups of the dye molecule and the positively charged Ca^{2+} site of HA. The dipole-dipole hydrogen bonding interaction exists between hydroxyl groups of HA and the azoic group of dye molecule. Also electrostatic interaction may occur between the cationic groups of dye such as Na^+ with anionic groups of apatite such as OH^- and PO_4^{3-} [28, 29]. In Y-HA, in addition to these interactions existence of Y^{3+} and O^{2-} sites further enhances the interactions. At lower pH, H^+ may compete with dye ions for the adsorption sites thereby inhibiting the adsorption of dyes. Similarly the adsorbed dye molecules act as a shield against further diffusion of acidic group and dissolution of apatite. Thus the increased dye adsorption of Y-HA can be attributed to the enhanced specific surface area and increased adsorption sites.

The regeneration ability of calcium phosphate adsorbents for reuse, inexpensive way of disposal after use without any environmental issues and the economic way of producing the adsorbents are the benefits of HA adsorbents [30, 31]. Also the efficiency of dye adsorption of HA can be improved by tailoring the properties.

Conclusion

RR 198 dye adsorption from aqueous solution has been studied using nanoparticles of HA and trivalent cation (yttrium) substituted HA. Y-HA showed an enhanced dye adsorption affinity due to the existence of additional adsorption sites owing to the difference in the oxidation state of substituent and its associated charge balance. Tuning the adsorption properties of the cost effective and regeneratable adsorbent HA can be achieved by the substitution of divalent cation by a trivalent cation. Also the nanocrystalline form of HA can be easily synthesized from various naturally occurring sources.

References
1. Kumar A., Chaudhary P., Verma P, *Sch. J. app. med. Sci.* 1(2)(2013)111.
2. Stergiopoulos D., Dermentzis K., Giannakoudakis P., Sotiropoulos S., *Global NEST Journal.* 16(3) (2014) 499.
3. Vijayaraghavan G., Shanthakumar S., J. Mater. Environ. Sci. 6 (6) (2015) 1672.
4. Fettouche S., Tahiri M., Madhouni R., Cherkaoui O., J. Mater. Environ. Sci. 6 (1) (2015) 129.
5. Amrhar O., Nassali H., Elyoubi M.S., J. Mater. Environ. Sci. 6 (11) (2015) 3054.
6. Rashed M.N., *Adsorption technique for the removal of organic pollutants from water and wastewater, organic pollutants - monitoring, risk and treatment,* (Ed: Prof. Rashed M.N), Intech, 2013, ch.7, pp.167-194.

7.   Ali I., Asim M., Khan T.A., *J. Environ. Manage.*113 (2012) 170.

8.   Qu X., Alvarez P J., Li Q., *Water Res*. 47 (2013) 3931.

9.   Amin M. T., Alazba A. A., Manzoor U., *Adv Mater Sci Eng*. (2014) 1.

10. Tiselius A., Hjerten S., Levin O., *Arch. Biochem. Biophys*. 66 (1956) 132.

11. Zhou H., Wu T., Dong X., Wang Q., Shen J., *Biochem. Biophys. Res. Commu.*361(2007) 91.

12. Hayakawa S., Kusudo Y., Takemoto S., Tsuru K., Osaka A., *Bioceramics: Mater Appl IV*, (Ed: Sundar V, Rusin R.P., Rutiser C.A), John Wiley & Sons, Inc., Hoboken, NJ, USA, 2012, Vol. 147, pp.111-119.

13. Corami A., Mignardi S., Ferrini V., *J. Colloid Interface Sci.* 317 (2008) 402.

14. Sairam Sundaram C., Viswanathan N., Meenakshi S., *J. Hazard. Mater.*155 (2008) 206.

15. Constantin L.V., Iconaru S., Ciobanu C.S., *Romanian Rep. Phys.*64 (2012) 788.

16. Hayakawa S., Ando K., Tsuru K., Osaka A., Fujii E., Kawabata K., Bonhomme C., Babonneau F., *J. Am. Ceram. Soc.* 90(2) (2007)565.

17. Liu G., Talley J.W., Na C., Larson S.L., Wolfe L.G., *Environ. Sci. Technol*. 44 (2010) 1366.

18. Liang C.H, Li F.B., Liu C.S., Lu J.L., Wang X.G., *Dyes and Pigments*, 76 (2008) 477.

19. Wang L., Li J., Wang Y., Zhao L., *Journal of Hazardous Materials*. 196(2011) 342.

20. Umoren S. A., Etim U. J., Israel A. U., J. Mater. Environ. Sci. 4 (1) (2013) 75.

21. Jenkins R., Snyder R.L., *X-ray Powder Diffractometry. An Introduction*. (Ed: Cernik R. J), John Wiley & Sons, New York, 2006, Vol.138, pp.1417-1418.

22. Joseph Nathanael A., Mangalaraj D., Hong S.I., Masuda Y., *Mater. Charact.*62 (2011) 1109.

23. Toker S. M., Tezcaner A., Evis Z., *J Biomed Mater Res B Appl Biomater*. 96B (2011) 207.

24. Ergun C., Webster TJ., Bizios R., Doremus RH., *J Biomed Mater Res.*59 (2002) 305.

25. Wei X., Fu C., Savino K., Yates M.Z., *Cryst. Growth Des*. 12 (2012) 217.

26. Ben Moussa S., Bachoua H., Badraoui B ., Fatteh N., *J. Mater. Environ. Sci.* 7 (5) (2016) 1810.

27. Yuen C.W.M., Ku S.K.A., Choi P.S.R., Kan C.W., Tsang S.Y., *RJTA*.9 (2005) 26.

28. Kandori K., Toshima S., Wakamura M., Fukusumi M., Morisada Y., *J. Phys. Chem. B*. 114 (2010) 2399.

29. Bell L. C., Posner A. M., Quirk J. P., *Nature*.239 (1972) 515.

30. Foo K.Y., Hameed B.H., *Chem. Eng. J*. 156 (2010) 2.

31. El Boujaady H., Mourabet M., EL Rhilassi A., Bennani-Ziatni M., El Hamri R., Taitai A**.,** *J. Mater. Environ. Sci.* 7 (11) (2016) 4049.

32. Dorozhkin S.V., *J. Colloid Interface Sci*. 191 (1997) 489.

33. Dorozhkin S.V., *World J Methodol*. 26(2012) 1.

34. Suteu D., Zaharia C., Malutan T., *J. Serb. Chem. Soc.* 76 (4) (2011) 607.

35. Wen YZ., Liu WQ., Fang ZH., Liu WP., *J Environ Sci.(China)*17 (2005) 766.

36. Ciobanu, G., Harja, M., Rusu, L. Mocanu, A.M., Luca, C., *Korean J. Chem. Eng.* 31(6) (2014) 1021.

(2017) ; http://www.jmaterenvironsci.com